Gaps and tails in graphene and graphane

B. Dóra, Klaus G. Ziegler

Angaben zur Veröffentlichung / Publication details:

Dóra, B., and Klaus G. Ziegler. 2009. "Gaps and tails in graphene and graphane." *New Journal of Physics* 11 (9): 095006. https://doi.org/10.1088/1367-2630/11/9/095006.

Gaps and tails in graphene and graphane

New Journal of Physics
The open-access journal for physics

Gaps and tails in graphene and graphane

B Dóra[1] **and K Ziegler**[2,3]

[1] Max-Planck-Institut für Physik Komplexer Systeme, Nöthnitzer Strasse 38, 01187 Dresden, Germany
[2] Institut für Physik, Universität Augsburg, D-86135 Augsburg, Germany
E-mail: klaus.ziegler@physik.uni-augsburg.de

New Journal of Physics **11** (2009) 095006 (16pp)
Received 15 May 2009
Published 30 September 2009
Online at http://www.njp.org/
doi:10.1088/1367-2630/11/9/095006

Abstract. We study the density of states (DOS) in monolayer and bilayer graphene in the presence of a random potential that breaks sublattice symmetries. While a uniform symmetry-breaking potential (SBP) opens a uniform gap, a random SBP also creates tails in the DOS. The latter can close the gap again, preventing the system from becoming an insulator. However, for a sufficiently large gap the tails contain localized states with nonzero DOS. These localized states allow the system to conduct at nonzero temperature via variable-range hopping. This result is in agreement with recent experimental observations in graphane by Elias *et al* (2009 *Science* **323** 610).

[3] Author to whom any correspondence should be addressed.

Contents

1. Introduction

Graphene is a single sheet of carbon atoms that forms a honeycomb lattice (HCL). A graphene monolayer as well as a stack of two graphene sheets (i.e. a graphene bilayer) are semimetals with remarkably good conducting properties [1]–[3]. These materials have been experimentally realized with external gates, which allow for a continuous change in the charge-carrier density. There exists a nonzero minimal conductivity at the charge neutrality point. Its value is very robust and almost unaffected by disorder or thermal fluctuations [3]–[6].

Many potential applications of graphene require an electronic gap to switch between conducting and insulating states. A successful step in this direction has been achieved by recent experiments with hydrogenated graphene (graphane) [7] and with gated bilayer graphene (BLG) [8]–[10]. These experiments take advantage of the fact that the breaking of a discrete symmetry of the lattice system opens a gap in the electronic spectrum at the Fermi energy. In the case of monolayer graphene (MLG), a staggered potential that depends on the sublattice of the HCL plays the role of such symmetry-breaking potential (SBP). For BLG, a gate potential that distinguishes between the two graphene layers plays a similar role.

With these opportunities one enters a new field in graphene, where one can switch between conducting and insulating regimes of a two-dimensional (2D) material, either by a chemical process (e.g. oxidation or hydrogenation) or by applying an external electric field [11].

The opening of a gap can be observed experimentally either by a direct measurement of the density of states (DOS) (e.g. by scanning tunneling microscopy [12]) or indirectly by measuring transport properties. In the gapless case, we observe a metallic conductivity $\sigma \propto \rho D$, where D is the diffusion coefficient (which is proportional to the scattering time) and ρ is the DOS. This gives typically a conductivity of the order of e^2/h. The gapped case, on the other hand, has a strongly temperature-dependent conductivity due to thermal activation of charge carriers [13]

$$\sigma(T) = \sigma_0 \, \mathrm{e}^{-T_0/T}, \tag{1}$$

with some characteristic temperature scale T_0, which depends on the underlying model. A different behavior was found experimentally in the insulating phase of graphane [7]:

$$\sigma(T) \approx \sigma_0 \, \mathrm{e}^{-(T_0/T)^{1/3}}, \tag{2}$$

which is known as 2D variable-range hopping [14]. This behavior indicates the existence of well-separated localized states, even at the charge-neutrality point, where the parameter T_0 depends on the DOS at the Fermi energy E_F as $T_0 \propto 1/\rho(E_\mathrm{F})$.

The experimental observation of a metal–insulator transition in graphane raises two questions: (i) what are the details that describe the opening of a gap and (ii) what is the DOS in the insulating phase? In this paper, we will focus on the mechanism of the gap opening due to an SBP in MLG and BLG. It is crucial for our study that the SBP is not uniform in the realistic 2D material. One reason for the latter is the fact that graphene is not flat but forms ripples [15]–[17]. Another reason is the incomplete coverage of a graphene layer with hydrogen atoms in the case of graphane [7]. The spatially fluctuating SBP leads to interesting effects, including a second-order phase transition due to spontaneous breaking of a discrete symmetry and the formation of Lifshitz tails.

2. Model

Quasiparticles in MLG or in BLG are described in tight-binding approximation by a nearest-neighbor hopping Hamiltonian

$$\mathbf{H} = -\sum_{\langle r,r'\rangle} t_{r,r'} c_r^\dagger c_{r'} + \sum_r V_r c_r^\dagger c_r + \mathrm{h.c.}, \tag{3}$$

where $c_r^\dagger$ (c_r) are fermionic creation (annihilation) operators at lattice site r. The underlying lattice structure is either an HCL (MLG) or two HCLs with Bernal stacking (BLG) [11, 18]. We have an intralayer hopping rate t and an interlayer hopping rate $t_\perp$ for BLG. There are different forms of the potential V_r, depending on whether we consider MLG or BLG. Here we begin with potentials that are uniform on each sublattice, whereas random fluctuations are considered in section 2.4.

2.1. MLG

V_r is a staggered potential with $V_\mathrm{r} = m$ on sublattice A and $V_\mathrm{r} = -m$ on sublattice B. This potential obviously breaks the sublattice symmetry of MLG. Such a staggered potential can be the result of chemical absorption of non-carbon atoms in MLG (e.g. oxygen or hydrogen [7]). A consequence of the symmetry breaking is the formation of a gap $\Delta_\mathrm{g} = m$. The spectrum of MLG consists of two bands with dispersion

$$E_k = \pm\sqrt{m^2 + \epsilon_k^2}, \tag{4}$$

where

$$\epsilon_k^2 = t^2[3 + 2\cos k_1 + 4\cos(k_1/2)\cos(\sqrt{3}k_2/2)] \tag{5}$$

for lattice spacing $a = 1$.

2.2. BLG

V_r is a biased gate potential that is $V_r = m$ ($V_r = -m$) on the upper (lower) graphene sheet. The potential in BLG has been realized as an external gate voltage, applied to the two layers of BLG [8]. The spectrum of BLG consists of four bands [11] with two low-energy bands

$$E_k^-(m) = \pm\sqrt{\epsilon_k^2 + t_\perp^2/2 + m^2 - \sqrt{t_\perp^4/4 + (t_\perp^2 + 4m^2)\epsilon_k^2}}, \tag{6}$$

where ϵ_k is the monolayer dispersion of equation (5), and two high-energy bands

$$E_k^+(m) = \pm\sqrt{\epsilon_k^2 + t_\perp^2/2 + m^2 + \sqrt{t_\perp^4/4 + (t_\perp^2 + 4m^2)\epsilon_k^2}}\,. \tag{7}$$

The spectrum of the low-energy bands has nodes for $m = 0$, where $E_k^-(0)$ vanishes in a $(k - K)^2$ manner, where K is the position of the nodes, which are the same as those of a single layer. For small $m \ll t_\perp$, a Mexican hat structure develops around $k = K$, with local extremum in the low-energy band at $E_k^-(m) = \pm m$ and a global minimum/maximum in the upper/lower low-energy band at $E_k^-(m) = mt_\perp/\sqrt{t_\perp^2 + 4m^2}$.

For small gating potential $V_r = \pm m$, we can expand $E_k^-(m)$ under the square root near the nodes and get

$$E_k^-(m) \sim \pm\sqrt{[1 - 4\epsilon_k^2 t_\perp (t_\perp^2 + 4\epsilon_k^2)^{-1/2}]m^2 + E_k^-(0)^2}. \tag{8}$$

where $t_\perp$ apparently reduces the gap. Very close to the nodes we can approximate the factor in front of m^2 by 1 and obtain an expression similar to the dispersion of MLG: $E_k^-(m) \sim \pm\sqrt{m^2 + E_k^-(0)^2}$. Here we notice the absence of the Mexican hat structure in this approximation. The resulting spectra for MLG and BLG are shown in figure 1.

2.3. Low-energy approximation

The two bands in MLG and the two low-energy bands in BLG represent a spinor-1/2 wave function. This allows us to expand the corresponding Hamiltonian in terms of Pauli matrices σ_j as

$$H = h_1\sigma_1 + h_2\sigma_2 + m\sigma_3. \tag{9}$$

Near each node the coefficients h_j read in low-energy approximation [19]

$$h_j = i\nabla_j \ \text{(MLG)}, \quad h_1 = \nabla_1^2 - \nabla_2^2, \quad h_2 = 2\nabla_1\nabla_2 \ \text{(BLG)}, \tag{10}$$

where (∇_1, ∇_2) is the 2D gradient.

2.4. Random fluctuations

In a realistic situation the potential V_r is not uniform, neither in MLG nor in BLG, as discussed in the introduction. As a result, electrons experience a randomly varying potential V_r along each graphene sheet, and m in the Hamiltonian of equation (9) becomes a random variable in space

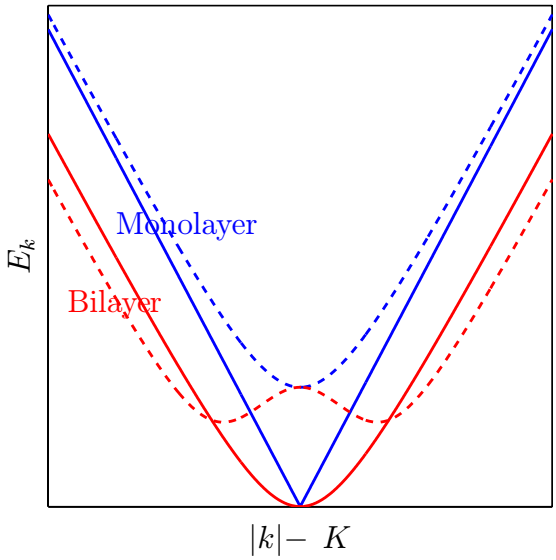

Figure 1. The energy spectra of MLG (blue) and BLG (red) are shown, with and without a gap (dashed and solid lines, respectively) for positive energies. Note the characteristic Mexican hat structure of gapped BLG.

as well. For BLG it is assumed that the gate voltage is adjusted at the charge-neutrality point such that on average m_r is exactly antisymmetric with respect to the two layers: $\langle m_1 \rangle_m = -\langle m_2 \rangle_m$.

At first glance, the Hamiltonian in equation (3) is a standard hopping Hamiltonian with random potential V_r. This is a model frequently used to study the generic case of Anderson localization [20]. The dispersion, however, is special in the case of graphene due to the HCL: at low energies it consists of two nodes (or valleys) K and K' [17, 19]. It is assumed here that randomness scatters only at small momentum such that intervalley scattering, which requires large momentum at least near the nodal points (NP), is not relevant and can be treated as a perturbation. Then each valley contributes separately to the DOS, and the contribution of the two valleys to the DOS ρ is additive: $\rho = \rho_K + \rho_{K'}$. This allows us to consider the low-energy Hamiltonian in equations (9) and (10), even in the presence of randomness for each valley separately. Within this approximation the term m_r is a random variable with mean value $\langle m_r \rangle_m = \bar{m}$ and variance $\langle (m_r - \bar{m})(m_{r'} - \bar{m}) \rangle_m = g\delta_{r,r'}$. The following analytic calculations will be based entirely on the Hamiltonian of equations (9) and (10) and the numerical calculations on the lattice Hamiltonian of equation (3). In particular, the average Hamiltonian $\langle H \rangle_m$ can be diagonalized by Fourier transformation and is

$$\langle H \rangle_m = k_1\sigma_1 + k_2\sigma_2 + \bar{m}\sigma_3 \tag{11}$$

for MLG with eigenvalues $E_k = \pm\sqrt{\bar{m}^2 + k^2}$. For BGL, the average Hamiltonian is

$$\langle H \rangle_m = (k_1^2 - k_2^2)\sigma_1 + 2k_1k_2\sigma_2 + \bar{m}\sigma_3 \tag{12}$$

with eigenvalues $E_k = \pm\sqrt{\bar{m}^2 + k^4}$.

2.5. Symmetries

Low-energy properties are controlled by the symmetry of the Hamiltonian and of the corresponding one-particle Green's function $G(\mathrm{i}\epsilon) = (H + \mathrm{i}\epsilon)^{-1}$. In the absence of sublattice-symmetry breaking (i.e. for $m = 0$), the Hamiltonian $H = h_1\sigma_1 + h_2\sigma_2$ has a continuous chiral symmetry

$$H \to \mathrm{e}^{\alpha\sigma_3} H \mathrm{e}^{\alpha\sigma_3} = H \tag{13}$$

with a continuous parameter α, since H anticommutes with σ_3. The term $m\sigma_3$ breaks the continuous chiral symmetry. However, the behavior under transposition $h_j^{\mathrm{T}} = -h_j$ for MLG and $h_j^{\mathrm{T}} = h_j$ for BLG in equation (10) provides a discrete symmetry:

$$H \to -\sigma_n H^{\mathrm{T}} \sigma_n = H, \tag{14}$$

where $n = 1$ for MLG and $n = 2$ for BLG. This symmetry is broken for the one-particle Green's function $G(\mathrm{i}\epsilon)$ by the $\mathrm{i}\epsilon$ term. To see whether or not the symmetry is restored in the limit $\epsilon \to 0$, the difference of $G(\mathrm{i}\epsilon)$ and the transformed Green's function $-\sigma_n G^{\mathrm{T}}(\mathrm{i}\epsilon)\sigma_n$ must be evaluated:

$$G(\mathrm{i}\epsilon) + \sigma_n G^{\mathrm{T}}(\mathrm{i}\epsilon)\sigma_n = G(\mathrm{i}\epsilon) - G(-\mathrm{i}\epsilon). \tag{15}$$

For the diagonal elements, this is the DOS at the NP $\rho(E = 0) \equiv \rho_0$ in the limit $\epsilon \to 0$. Thus, the order parameter for spontaneous symmetry breaking is ρ_0. According to the theory of phase transitions, the transition from a nonzero ρ_0 (spontaneously broken symmetry) to $\rho_0 = 0$ (symmetric phase) is a second-order phase transition, and should be accompanied by a divergent correlation length at the transition point. Since our symmetry is discrete, such a phase transition can exist in $d = 2$ and should be of Ising type. A calculation, using the self-consistent Born approximation (SCBA) of ρ_0, gives indeed a second-order transition at the point where ρ_0 vanishes with a divergent correlation length ξ for the DOS fluctuations

$$\xi \sim \xi_0 (m_{\mathrm{c}}^2 - \bar{m}^2)^{-1}$$

for $\bar{m}^2 \sim m_{\mathrm{c}}^2$ with a finite coefficient ξ_0 [21]. Whether or not this transition is an artifact of the SCBA or represents a physical effect due to the appearance of two types of spectra (localized for vanishing SCBA-DOS and delocalized for nonzero SCBA-DOS) is not obvious here and requires further studies.

2.6. DOS

Our focus in the subsequent calculation is on the DOS of MLG and BLG. In the absence of disorder, the DOS of 2D Dirac fermions opens a gap $\Delta \propto \bar{m}$ as soon as a nonzero term $\bar{m}$ appears in the Hamiltonian of equation (9), since the low-energy dispersion is $E_k = \pm\sqrt{\bar{m}^2 + k^2}$ for MLG and $E_k = \pm\sqrt{\bar{m}^2 + k^4}$ for BLG, respectively (cf figure 2). Here we evaluate the DOS of MLG and BLG in the presence of a uniform gap. Given the energy spectrum, the DOS is defined as

$$\rho(E) = \sum_k \delta(E - E_k). \tag{16}$$

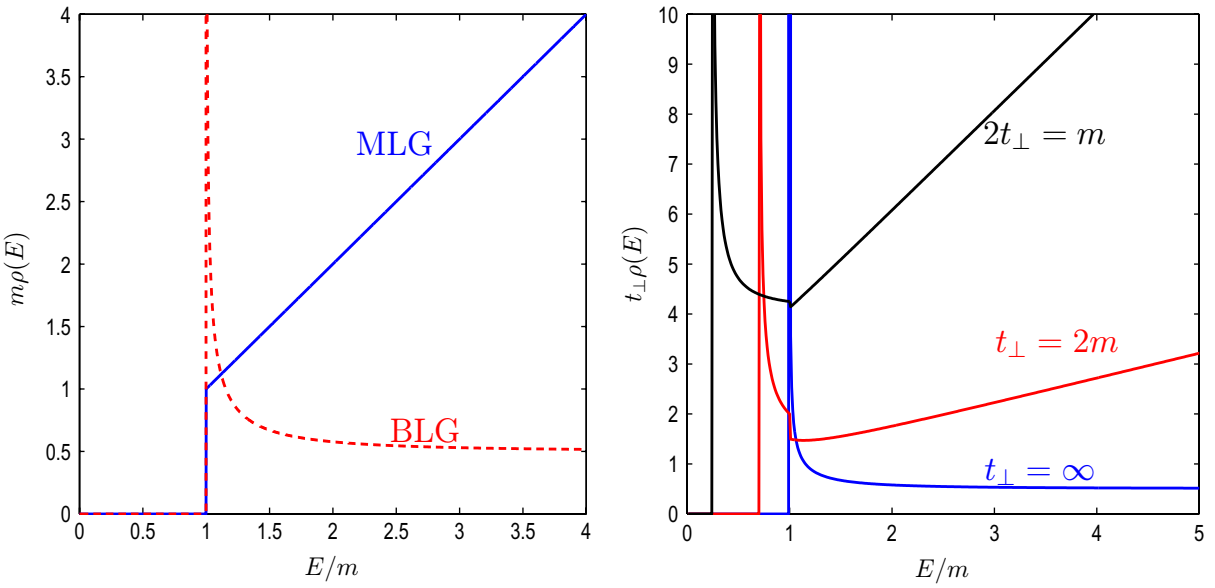

Figure 2. DOS for a uniform SBP for MLG and BLG is shown in the left panel. The DOS for a uniform SBP for BLG is shown for several values of $t_\perp$. For small $t_\perp$, the Mexican hat structure influences the DOS by shifting the gap to lower values, and by developing a kink at $E = m$.

By using the MLG dispersion, this reduces to

$$\rho(E) = |E|\Theta(|E| - m), \tag{17}$$

where $\Theta(x)$ is the Heaviside function. For BLG, this gives

$$\rho(E) = \frac{|E|}{2\sqrt{E^2 - m^2}}\Theta(|E| - m), \tag{18}$$

which are shown in figure 2. By retaining the full low-energy spectrum for BLG, E_k^-, the DOS can still be evaluated in a closed form, with the result

$$\rho(E) = |E| \begin{cases} \dfrac{(t_\perp^2 + 4m^2)}{\sqrt{(t_\perp^2 + 4m^2)E^2 - t_\perp^2 m^2}}, & \text{for } m > |E| > \dfrac{mt_\perp}{\sqrt{t_\perp^2 + 4m^2}}, \\ \dfrac{(t_\perp^2 + 4m^2)}{2\sqrt{(t_\perp^2 + 4m^2)E^2 - t_\perp^2 m^2}} + 1, & \text{for } |E| > m. \end{cases} \tag{19}$$

In the limit of $t_\perp \gg (E, m)$, this reduces to equation (18) after dividing it by $t_\perp$, which was set to 1 in the low-energy approximation, and the DOS saturates to a constant value after the initial divergence. For finite $t_\perp$, however, the Dirac nature of the spectrum appears again, and the high-energy DOS increases linearly even for the BLG, similarly to the MLG case. For $m = 0$ and $E \ll t_\perp$, this lengthy expression gives

$$\rho(E \ll t_\perp) = \frac{t_\perp}{2}. \tag{20}$$

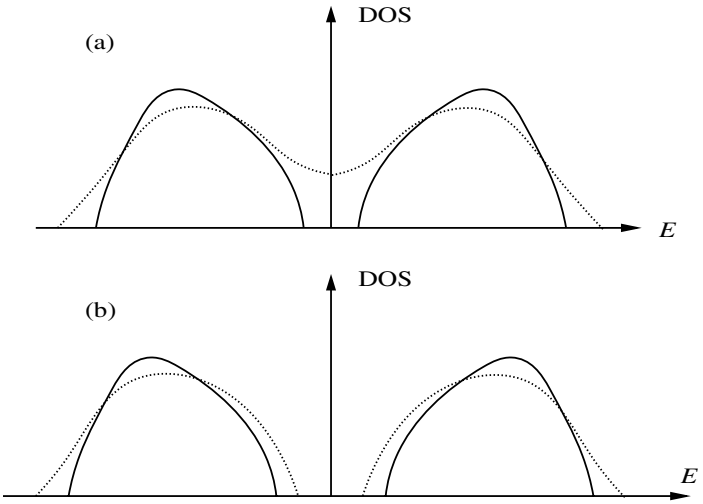

Figure 3. Schematic shape of the DOS: full curves are the bulk DOS for uniform SBP, dotted curves represent the broadening by disorder. The broadened DOS can overlap inside the gap for $\bar{m} < m_c$ (a) or not for $\bar{m} > m_c$ (b), depending on the average SBP $\bar{m}$. m_c is given in equation (29).

An interesting question, from the theoretical as well as from the experimental point of view, appears here: what is the effect of random fluctuations around $\bar{m}$? Previous calculations, based on the SCBA, have revealed that those fluctuations can close the gap again, even for an average SBP term $\bar{m} \neq 0$ [22]. Only if $\bar{m}$ exceeds a critical value m_c (which depends on the strength of the fluctuations), an open gap was found in these calculations (cf figure 3). This describes a special transition from metallic to insulating behavior. In particular, the DOS at the Dirac point ρ_0 vanishes with $\bar{m}$ like a power law

$$\rho_0(\bar{m}) \sim \sqrt{\bar{m} - m_c^2}. \tag{21}$$

The exponent $1/2$ of the power law is probably an artifact of the SCBA, similar to the critical exponent in mean-field approximations.

3. SCBA

The average one-particle Green's function can be calculated from the average Hamiltonian $\langle H \rangle_m$ by employing the SCBA [23]–[25]

$$\langle G(\mathrm{i}\epsilon) \rangle_m \approx (\langle H \rangle_m + \mathrm{i}\epsilon - 2\Sigma)^{-1} \equiv G_0(\mathrm{i}\eta, m_s). \tag{22}$$

The SCBA is also known as the self-consistent non-crossing approximation in the Kondo and superconducting community. The self-energy Σ is a 2×2 tensor due to the spinor structure of the quasiparticles: $\Sigma = -(\mathrm{i}\eta\sigma_0 + m_s\sigma_3)/2$. Scattering by the random SBP produces an

imaginary part of the self-energy η (i.e. a one-particle scattering rate) and a shift m_s of the average SBP $\bar{m}$ (i.e. $\bar{m} \to m' \equiv \bar{m} + m_s$). Σ is determined by the self-consistent equation

$$\Sigma = -g\sigma_3(\langle H\rangle_m + i\epsilon - 2\Sigma)^{-1}_{rr}\sigma_3 \,. \tag{23}$$

The symmetry in equation (14) implies that with Σ also

$$\sigma_n \Sigma \sigma_n = -(i\eta\sigma_0 - m_s\sigma_3)/2 \tag{24}$$

is a solution (i.e. $m_s \to -m_s$ creates a second solution).

The average DOS at the NP is proportional to the scattering rate: $\rho_0 = \eta/2g\pi$. This reflects that scattering by the random SBP creates a nonzero DOS at the NP if $\eta > 0$.

Now we assume that the parameters η and m_s are uniform in space. Then equation (23) can be written in terms of two equations, one for the one-particle scattering rate η and another for the shift of the SBP m_s, as

$$\eta = gI\eta, \quad m_s = -\bar{m}gI/(1+gI), \tag{25}$$

where I is a function of $\bar{m}$ and η and also depends on the Hamiltonian. For MLG it reads with momentum cutoff λ

$$I_{\mathrm{MLG}} = \frac{1}{2\pi}\ln\left[1 + \frac{\lambda^2}{\eta^2 + (\bar{m}+m_s)^2}\right] \tag{26}$$

and for BLG

$$I_{\mathrm{BLG}} \sim \frac{1}{4\sqrt{\eta^2 + (\bar{m}+m_s)^2}} \quad (\lambda \sim \infty). \tag{27}$$

A nonzero solution η requires $gI = 1$ in the first part of equation (25), such that $m_s = -\bar{m}/2$ from the second part. Since the integrals I are monotonically decreasing functions for large $\bar{m}$, a real solution with $gI = 1$ exists only for $|\bar{m}| \leqslant m_c$. For both MLG and BLG, the solutions read

$$\eta^2 = (m_c^2 - \bar{m}^2)\Theta(m_c^2 - \bar{m}^2)/4, \tag{28}$$

where the model dependence enters only through the critical average SBP m_c:

$$m_c = \begin{cases} (2\lambda/\sqrt{e^{2\pi/g}-1}) \sim 2\lambda e^{-\pi/g}, & \text{MLG}, \\ g/2, & \text{BLG}. \end{cases} \tag{29}$$

Here m_c is much bigger for BGL, a result that indicates that the effect of disorder is much stronger in BLG. This is also reflected by the scattering rate at $\bar{m} = 0$, which is $\eta = m_c/2$.

A central assumption of the SCBA is a uniform self-energy Σ. The imaginary part of Σ is the scattering rate η, created by the random fluctuations. Therefore, a uniform η means that effectively random fluctuations are densely filling the lattice. If the distribution of the fluctuations is too dilute, however, there is no uniform nonzero solution of equation (23). Nevertheless, a dilute distribution can still create a nonzero DOS, as we will discuss in the following: we study contributions to the DOS due to rare events, leading to Lifshitz tails.

4. Lifshitz tails

In the system with uniform SBP, the gap can be destroyed locally by a local change of the SBP $m \to m + \delta m_r$ due to the creation of a bound state. We start with a translational-invariant system and add δm_r on site r. To evaluate the corresponding DOS from Green's function $G = (H + \mathrm{i}\epsilon + \delta m \sigma_3)^{-1}$, using Green's function $G_0 = (H + \mathrm{i}\epsilon)^{-1}$ with uniform m, we employ the lattice version of the Lippmann–Schwinger equation [26]

$$G = G_0 - G_0 T_S G_0 = (\mathbf{1} - G_0 T_r) G_0, \tag{30}$$

with the 2×2 scattering matrix

$$T_r = (\sigma_0 + \delta m_r \sigma_3 G_{0,rr})^{-1} \sigma_3 \delta m_r. \tag{31}$$

In the case of MLG, we have

$$G_0 = [(E + \mathrm{i}\epsilon)\sigma_0 - m\sigma_3] \frac{1}{2\pi} \int_0^\lambda \frac{k}{(\epsilon - \mathrm{i}E)^2 + m^2 + k^2} \mathrm{d}k \tag{32}$$

$$\sim (E\sigma_0 - m\sigma_3) \frac{1}{4\pi} \log[1 + \lambda^2/(m^2 - E^2)] + o(\mathrm{i}\epsilon) \equiv (g_0 + \mathrm{i}\epsilon s)\sigma_0 + g_3\sigma_3. \tag{33}$$

(Remark: the DOS of BLG has the same form.) Then the imaginary part of the Green's function reads

$$\mathrm{Im}[G(\eta)] = -\begin{pmatrix} \delta_{\epsilon s}(g_0 + g_3 + \delta m_r) & 0 \\ 0 & \delta_{\epsilon s}(g_0 - g_3 - \delta m_r) \end{pmatrix}, \tag{34}$$

with

$$\delta_{\epsilon s}(x) = \frac{\epsilon s}{x^2 + \epsilon^2 s^2}. \tag{35}$$

Thus, the DOS is the sum of two Dirac delta peaks

$$\rho_r \propto \delta_{\epsilon s}(g_0 + g_3 + \delta m_r) + \delta_{\epsilon s}(g_0 - g_3 - \delta m_r). \tag{36}$$

The Dirac delta peak appears with probability $\propto \exp(-(g_0 \pm g_3)^2/g)$ for a Gaussian distribution. This calculation can easily be generalized to δm_r on a set of several sites r [26]. Then the appearance of several Dirac delta peaks decreases exponentially. Moreover, these contributions are local and form localized states. For stronger fluctuations δm_r (i.e. for increasing g), the localized states can start to overlap. This is a quantum analogue of classical percolation.

The localized states in the Lifshitz tails can be taken into account by a generalization of the SCBA to non-uniform self-energies. The main idea is to search for space-dependent solutions Σ_r of equation (23). In general, this is a difficult problem. However, we have found that this problem simplifies essentially when we study it in terms of a $1/\bar{m}$ expansion. Using a Gaussian distribution, this method gives Lifshitz tails of the form [27]:

$$\rho_0(\bar{m}) \sim \frac{\bar{m}^4}{32\sqrt{\pi} g^{5/2}} \mathrm{e}^{-\bar{m}^2/4g}. \tag{37}$$

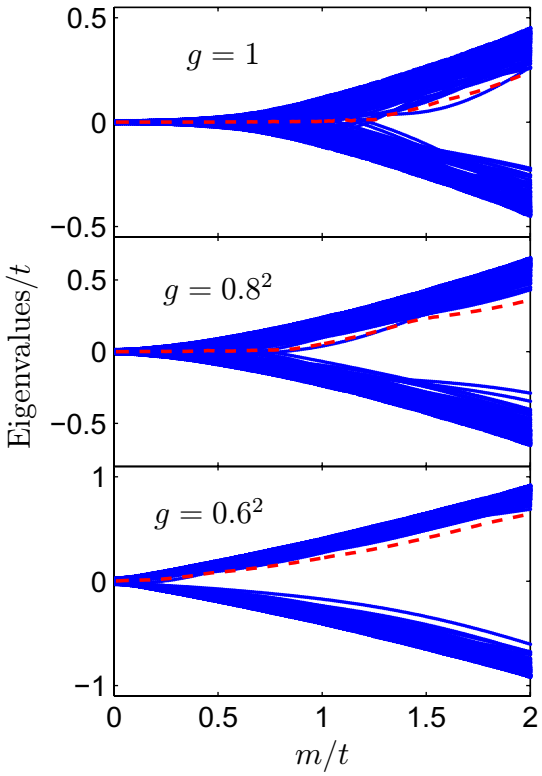

Figure 4. The evolution of the 200 lowest eigenvalues is shown for a given random mass configuration with Gaussian distribution (with variance g) on a 600×600 HCL, by varying the uniform gap. The red line denotes the maximum of the level spacing of these eigenvalues, a possible definition of the average gap.

5. Numerical approach

To understand the behavior of random gap fluctuations in graphene and also the limitations of the SCBA, we carried out extensive numerical simulations on the HCL, allowing for various random gap fluctuations on top of a uniform gap $\bar{m}$. These fluctuations are simulated by box and Gaussian distributions. From the SCBA, the emergence of a second-order phase transition at a critical mean m_c is obvious for a given variance. This is best manifested in the behavior of the DOS, which stays finite for $(\bar{m}) < m_c$, and vanishes afterwards, and serves as an order parameter. Does this picture indeed survive, when higher order corrections in the fluctuations are taken into account?

To start with, we take a fix random mass configuration with a given variance and the HCL with the conventional hoppings (t), represented by H_0. Then, we take a separate Hamiltonian, responsible for the uniform, non-fluctuating gaps, denoted by H_{gap}, and study the evolution of the eigenvalues of $H_0 + \bar{m} H_{\text{gap}}$ by varying $\bar{m}$ for a 600×600 lattice. By using Lanczos diagonalization, we focus our attention only to the 200 eigenvalues closest to the NP. Their evolution is shown in figure 4. This supports the existence of a finite m_c, but since it originates from a single random disorder configuration, rare events can alter the result. As a possible definition of the rigid gap, we also show the maximum of the energy level spacing for these

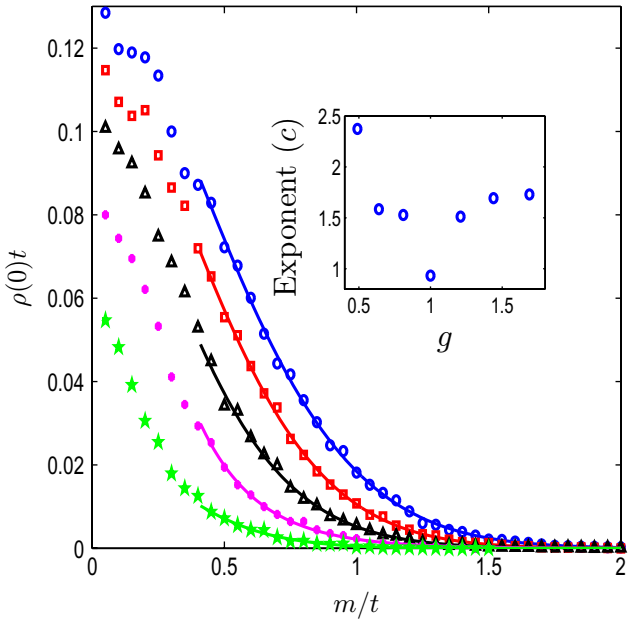

Figure 5. The DOS at the NP is plotted for Gaussian distribution for a 200×200 HCL for $g = 0.9^2$, 1, 1.1^2, 1.2^2 and 1.3^2 from bottom to top after 400 averages. The symbols denote the numerical data, solid lines are fits using $a \exp(-bm^c)$. The inset shows the obtained exponents, c, as a function of g, which is close to 1.5.

eigenvalues as a function of $\bar{m}$. As seen, it starts to increase abruptly at a certain value of $\bar{m}$, which can define m_c.

To investigate whether a finite critical m_c survives, we take smaller systems and evaluate the averaged DOS directly from many disorder realizations. To achieve this, we take a 200×200 HCL, and evaluate the 200 closest eigenvalues to the NP, and count their number in a given small interval, ΔE (smaller than the maximal eigenvalues) around zero. This method was found to be efficient in studying other types of randomness [28]. We mention that large values of ΔE take contribution from higher energy states into account, while too small values are sensitive to the discrete lattice and consequently the discrete eigenvalue structure of the Hamiltonian. For lattices containing a few 10^4–10^5 sites, $\Delta E/t \sim 10^{-2}$–10^{-4} are convenient.

The resulting DOS is plotted in figures 5 and 6 for Gaussian (with variance g) and box distribution (within $[-W \ldots W]$, variance $g = W^2/3$). This does not indicate a sharp threshold, but rather the development of long Lifshitz tails due to randomness, as we already predicted in the previous section. To analyze them, we fitted the numerical data by assuming exponential tails of the form

$$\rho(0) = t \exp(-a - bm^c) \tag{38}$$

for a Gaussian and

$$\rho(0) = t \exp(-a - b/|\bar{m} - W|^c) \tag{39}$$

for a box distribution, as suggested by Cardy [29]. The obtained c values are visualized in the insets of figures 5 and 6. Given the good agreement, we believe that the DOS at the NP is made

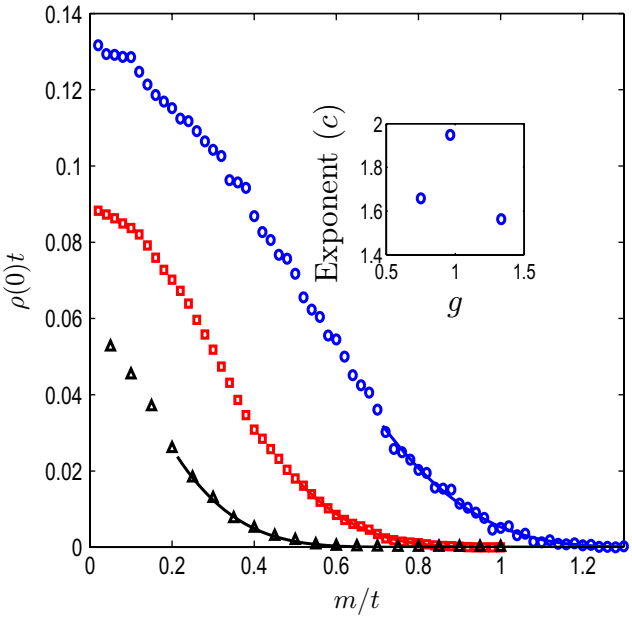

Figure 6. The DOS at the NP is plotted for box distributed ($[-W \ldots W]$) randomness for a 200×200 HCL for $W = 1.5$, 1.7 and 2 ($g = W^2/3$) from bottom to top after 400 averages. The symbols denote the numerical data, solid lines are fits using $a \exp(-b/|\bar{m} - W|^c)$. The inset shows the obtained exponents, c, as a function of g.

of states that are localized in a Lifshitz tail. We mention that these results are not sensitive to finite size scaling at these values of the disorder and uniform gap, only smaller systems (like the 30×30 HCL) require more averages ($\sim 10^4$), whereas for larger ones (such as the 200×200 with 400 averages) fewer averages are sufficient.

In figure 7, the energy-dependent DOS is shown for Gaussian distribution with $g = 1$ and for several uniform gap values. With increasing $\bar{m}$, the DOS diminishes rapidly at low energies and develops a pseudogap. The logarithmic singularity at $E = t$ is washed out for $g = 1$. We also show the inverse of the DOS, proportional to T_0, the characteristic temperature scale of variable range hopping as a function of the carrier density (which is proportional to E^2).

6. Discussion

MLG and BLG consist of two bands that touch each other at two NP (or valleys). Near the nodes the spectrum of MLG is linear (Dirac-like) and the spectrum of BLG is quadratic. The application of a uniform SBP opens a gap in the DOS for both cases. For a random SPB, however, the situation is less obvious. First of all, it is clear that randomness leads to a broadening of the bands. If we have two separate bands due to a small uniform SPB, randomness can close the gap again due to broadening (cf figure 3). The broadening of the bands depends on the strength of the fluctuations of the random SBP. In the case of a Gaussian distribution there are energy tails for all energies.

Now we focus on the NP, i.e. we consider $E = 0$ and ρ_0. Then we have two parameters in order to change the gap structure: the average SBP $\langle m \rangle \equiv \bar{m}$ and the variance g. $\bar{m}$ allows us

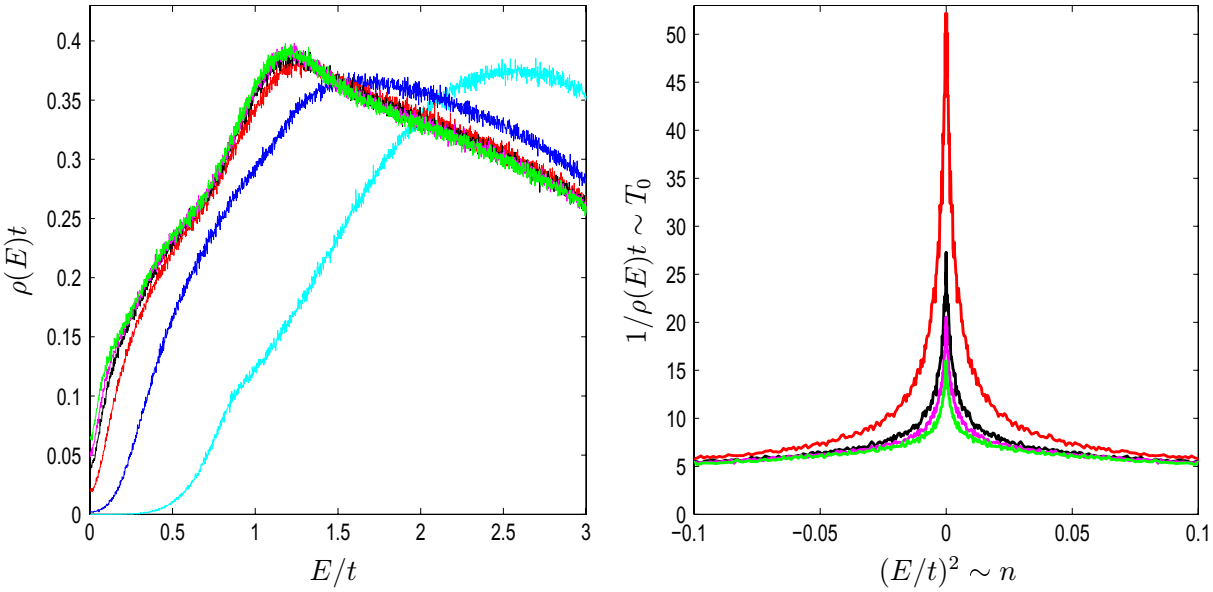

Figure 7. The energy-dependent DOS is plotted for Gaussian distribution for a 30×30 HCL after 10^4 averages for $g = 1$, $m = 2$ (cyan), 1 (blue), 0.5 (red), 0.3 (black), 0.2 (magenta) and 0 (green) in the left panel. The right panel visualizes the inverse of the DOS, being proportional to T_0 in the variable range hopping model as a function of the energy squared (proportional to the carrier density).

to broaden the gap and g has the effect of closing it due to broadening of the two subbands. Previous calculations have shown that at the critical value $m_c(g)$ of equation (29) the metallic behavior breaks down for $\bar{m} > m_c(g)$ [22]. On the other hand, Gaussian randomness creates tails at all energies. Consequently, there are localized states for $|\bar{m}| \geqslant m_c(g)$ at the NP, and there are delocalized states for $|\bar{m}| < m_c(g)$ at the NP. The localized states in the tails are described, for instance, by the Lippmann–Schwinger equation (30). The SCBA with uniform self-energy is not able to produce the localized tails. An extension of the SCBA with non-uniform self-energies provides localized tails although, as an approximation for large $\bar{m}$ has shown [27]. This is also in good agreement with our exact diagonalization of finite systems up to 200×200 size.

A possible interpretation of these results is that there are two different types of spectra. In a special realization of m_r the tails of the DOS represent localized states. On the other hand, the DOS at the NP $E = 0$, obtained from the SCBA with *uniform* self-energy, comes from extended states [22]. The localized and the delocalized spectrum separate at the critical value m_c, undergoing an Anderson transition.

Conductivity. Transport, i.e. the metallic regime, is related to the DOS through the Einstein relation $\sigma \propto \rho D$, where D is the diffusion coefficient. The latter was found in [22] for $E \sim 0$ as

$$D = \frac{ag\sqrt{m_c^2 - \bar{m}^2}}{2\pi m_c^2}\Theta(m_c^2 - \bar{m}^2), \tag{40}$$

where $a = 1$ ($a = 2$) for MLG (BLG). Together with the DOS $\rho_0 = \eta/2g\pi$ and the scattering rate η in equation (28), the Einstein relation gives us at the NP

$$\sigma(\omega \sim 0) \propto \rho_0 D \frac{e^2}{h} \approx \frac{a}{8\pi^2}\left(1 - \frac{\bar{m}^2}{m_c^2}\right)\Theta(m_c^2 - \bar{m}^2)\frac{e^2}{h}. \tag{41}$$

In the localized regime (i.e. for $|\bar{m}| \geqslant m_c$), the conductivity is nonzero only for positive temperatures $T > 0$. Then we can apply the formula for variable-range hopping in equation (2), which fits well the experimental result in graphane of [7]. The parameter T_0 is related to the DOS at the Fermi level as [14]

$$k_B T_0 \propto \frac{1}{\xi^2 \rho(E_F)}, \tag{42}$$

where ξ is the localization length. T_0 has its maximum at the NP $E_F = 0$, as shown in figure 7 and decreases monotonically with increasing carrier density, as in the experiment on graphane [7].

In conclusion, we have studied the DOS in MLG and BLG at low energies in the presence of a random SBP. While a uniform SBP opens a uniform gap, a random SBP also creates tails in the DOS. The latter can close the gap again, preventing the system to become an insulator at the nodes. However, for a sufficiently large gap the tails contain localized states with nonzero DOS. These localized states allow the system to conduct at nonzero temperature via variable-range hopping. This result is in agreement with recent experimental observations [7].

Acknowledgments

This work was supported by a grant from the Deutsche Forschungsgemeinschaft and by the Hungarian Scientific Research Fund under grant number K72613.

References

[1] Novoselov K S, Geim A K, Morozov S V, Jiang D, Katsnelson M I, Grigorieva I V, Dubonos S V and Firsov A A 2005 *Nature* **438** 197
[2] Zhang Y, Tan Y-W, Stormer H L and Kim P 2005 *Nature* **438** 201
[3] Geim A K and Novoselov K S 2007 *Nat. Mater.* **6** 183
[4] Tan Y-W, Zhang Y, Bolotin K, Zhao Y, Adam S, Hwang E H, Das Sarma S, Stormer H L and Kim P 2007 *Phys. Rev. Lett.* **99** 246803
[5] Chen J H, Jang C, Fuhrer M S, Williams E D and Ishigami M 2008 *Nat. Phys.* **4** 377
[6] Morozov S V, Novoselov K S, Katsnelson M I, Schedin F, Elias D C, Jaszczak J A and Geim A K 2008 *Phys. Rev. Lett.* **100** 016602
[7] Elias D C *et al* 2009 *Science* **323** 610
[8] Taisuke O, Bostwick A, Seyller T, Horn K and Rotenberg E 2006 *Science* **313** 951
[9] Oostinga J B, Heersche H B, Liu X, Morpurgo A F and Vandersypen L M K 2008 *Nat. Mater.* **7** 151
[10] Gorbachev R V, Tikhonenkoa F V, Mayorova A S, Horsella D W and Savchenkoa A K 2008 *Physica* E **40** 1360
[11] Castro E V, Peres N M R, Lopes dos Santos J M B, Guinea F and Castro Neto A H 2008 *J. Phys.: Conf. Ser.* **129** 012002
[12] Li G, Luican A and Andrei E Y 2009 *Phys. Rev. Lett.* **102** 176804
[13] Mott N F 1990 *Metal–Insulator Transitions* (London: Taylor and Francis)

[14] Mott N F 1969 *Phil. Mag.* **19** 835
[15] Morozov S V *et al* 2006 *Phys. Rev. Lett.* **97** 016801
[16] Meyer J C *et al* 2007 *Nature* **446** 60
[17] Castro Neto A H, Guinea F, Peres N M R, Novoselov K S and Geim A K 2009 *Rev. Mod. Phys.* **81** 109
[18] McCann E and Fal'ko V I 2006 *Phys. Rev. Lett.* **96** 086805
McCann E 2006 *Phys. Rev.* B **74** 161403
[19] McCann E *et al* 2006 *Phys. Rev. Lett.* **97** 146805
[20] Anderson P W 1958 *Phys. Rev.* **109** 1492
[21] Ziegler K 1997 *Phys. Rev.* B **55** 10661
[22] Ziegler K 2009 *Phys. Rev. Lett.* **102** 126802
Ziegler K 2009 *Phys. Rev.* B **79** 195424
[23] Suzuura H and Ando T 2002 *Phys. Rev. Lett.* **89** 266603
[24] Peres N M R, Guinea F and Castro Neto A H 2006 *Phys. Rev.* B **73** 125411
[25] Koshino M and Ando T 2006 *Phys. Rev.* B **73** 245403
[26] Ziegler K 1985 *J. Phys. A: Math. Gen.* **18** L801
[27] Villain-Guillot S, Jug G and Ziegler K 2000 *Ann. Phys., LPZ.* **9** 27
[28] Ziegler K, Dóra B and Thalmeier P 2009 *Phys. Rev.* B **79** 235431
[29] Cardy J L 1978 *J. Phys. C: Solid State Phys.* **11** L321